Composites Science and Technology 175 (2019) 85–91

Contents lists available at ScienceDirect

Composites Science and Technology

journal homepage: www.elsevier.com/locate/compscitech

Thermally conductive nanostructured, aramid dielectric composite films with boron nitride nanosheets

Meiyan Lin, Yinghui Li, Ke Xu, Yanghao Ou, Lingfeng Su, Xiao Feng, Jun Li, Haisong Qi, Detao Liu*

State Key Laboratory of Pulp and Paper Engineering, South China University of Technology, Guangzhou 510640, PR China

ARTICLE INFO

Keywords:
A. aramid nanofibers
A. boron nitride nanosheets
B. thermal conductivity
B. dielectric

ABSTRACT

The rapid development of modern electronics and high-frequency and high-speed circuits sets stringent requirements of low dielectric permittivity and efficient heat removal of thermal-management materials to reduce the time delay of signal propagation and ensure the long lifetime of the electronics. In this work, we report a novel thermally conductive and minimally dielectric nanocomposite film by vacuum filtering aramid nanofibers (ANFs) on nylon filter with boron nitride nanosheets (BNNSs). To obtain a continuous, uniform, freestanding composite film with both low dielectric permittivity and strong thermal conductivity, ANF suspensions were dialyzed and then absorbed into a BNNSs/Isopropanol (IPA) dispersion by bath-sonication. The advantage of the nanocomposite film lies in that it possesses an out-plane thermal conductivity up to 0.6156 ($w{\cdot}m^{-1}{\cdot}k^{-1}$) at BNNSs mass percent of 50 wt%, a conductivity that is almost 5 times that of the pure nano-aramid film. The nanocomposite film also boasts a low dielectric permittivity (~2.4 at 10^8 Hz) along with excellent mechanical flexibility and strength (~62 MPa).

1. Introduction

Although miniaturization is one of the main developmental aspects of modern electronic and photonic devices, it inevitably gives rise to thermal failure and performance degradation due to intense heat generated by the components [1–3]. Therefore, the issue of heat dissipation becomes increasingly urgent as devices become smaller. However, in actual electronic applications, especially within the communications field, these materials not only require high thermal conductivity but also low dielectric permittivity so that they can be applied in high-frequency and high-speed communication devices [4–6]. Papery film, with good flexibility and excellent processability, is an emerging material for thermal management in electronics. Papery films with anisotropic thermal conductivity and desirable mechanical properties, which could dissipate heat from hot regions along the in-plane direction while preventing neighboring components from being influenced, are highly needed, particularly for portable and collapsible electronic devices [3,7,8]. Zhu et al. reported a nanocomposite paper with layered boron nitride nanosheets wired by nanofibrillated cellulose (NFC) that has superior thermal and mechanical properties [9]. Wu et al. reported a biodegradable and highly thermally conductive film, with an orderly structure and good strength and toughness, based on cellulose nanofibers (CNFs) and fluorinated boron nitride nanosheets (f-BNNSs) and prepared by simple vacuum-assisted filtration [10]. It is undoubted that the structure, built by layered boron nitride nanosheets (BNNSs) and nanocellulose, shows great abilities [11–13]. The BNNSs can tightly stack in the network structure formed by the nanocellulose while the layered structure remains well-preserved in the film, resulting in high thermal conductivity and desirable mechanical properties [9,14]. However, these materials derived from CNFs are not suitable for high-frequency and high-speed communication applications because of their material limitations in terms of dielectric constant and stability. To obtain a low dielectric film, aramid fiber is a superior material to prepare films with high tensile strength and low dielectric properties [15,16]. However, the structural size difference between the macro aramid fiber and the nanosheets make it unsuitable for the preparation of flexible, thermally conductive film or paper. Interestingly, Kotov's group has reported that aramid fibers could be split into aramid nanofibers (ANFs) completely in dimethyl sulfoxide (DMSO) with the presence of some potassium hydroxide (KOH) [17]. Cao et al. reported that ANFs can act as high-performance polymeric building blocks and form mechanically robust ANFs nanopapers [18]. Inspired by this, a macroscopic nanocomposite film with high thermal conductivity and low dielectric performance can be expected by combining ANFs and

* Corresponding author.
E-mail address: dtliu@scut.edu.cn (D. Liu).

https://doi.org/10.1016/j.compscitech.2019.02.006
Received 23 October 2018; Received in revised form 30 January 2019; Accepted 4 February 2019
Available online 07 February 2019

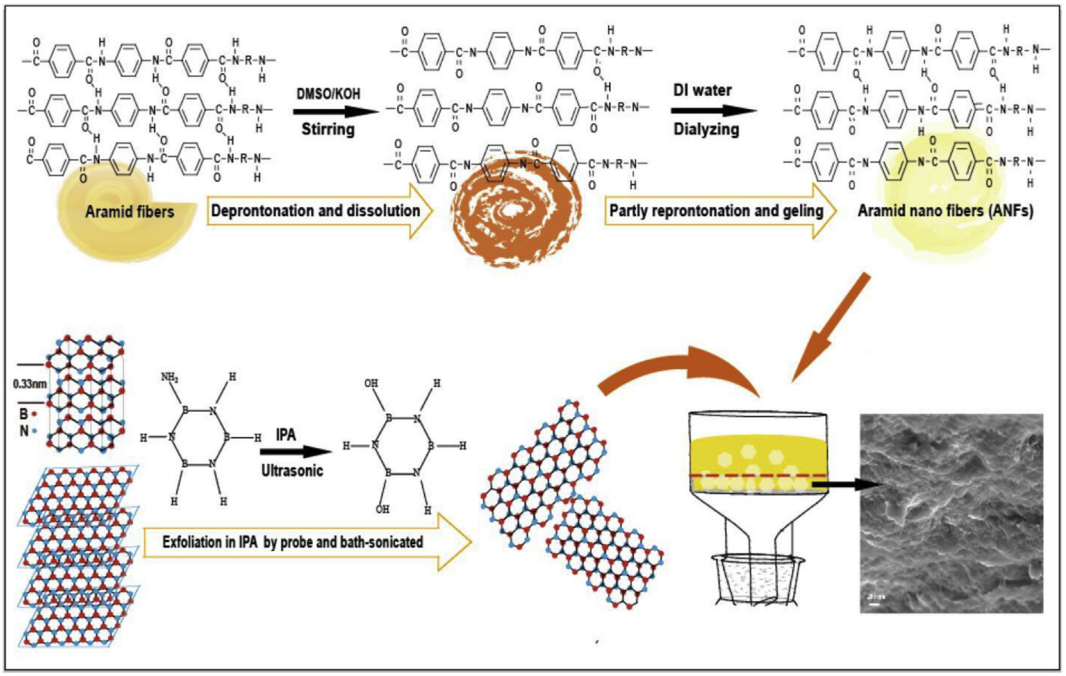

Fig. 1. Process for preparing nanocomposite films.

BNNSs. The ANFs can form a network structure and hold the BNNSs in the process of vacuum-assisted filtration as a new nanoscale component, which can produce composite membranes with high strength and thermal conductivity [19–21]. In this work, we report a novel nanocomposite film based on ANFs and BNNSs. The BNNSs are tightly stacked in the network structure formed by flocculated ANFs with the layered structure being well-preserved in the film (Fig. 1). Compared to that of the pure nano-aramid film, the thermal conductivity for the nanocomposite film with 50 wt% BNNSs increased to 0.6156 ($w{\cdot}m^{-1}{\cdot}k^{-1}$), almost 5 times that of the pure nano-aramid film. The nanocomposite film also boasts a low electric conductivity, dielectric permittivity and dissipation factor tan δ. In addition to good thermal conductivity, the excellent dielectric or insulated BNNSs/ANFs hybrid films also show excellent mechanical flexibility and strength.

2. Materials and methods

2.1. Materials

Para-aramid chopped fibers (ACFs) with average lengths between 5 and 6 mm were purchased from DuPont. Dimethyl sulfoxide (DMSO), potassium hydroxide (KOH), and isopropanol (IPA) were all purchased from Sigma-Aldrich and used as received. Hexagonal boron nitride powder (1–2 μm) was provided by Aladdin. DI water (18.2 MΩ/cm) was obtained from a Millipore Milli-Q system.

2.2. Preparation of boron nitride nanosheets dispersion (BNNSs)

According to Zhu's research and with some modifications, exfoliated BNNSs were prepared as follows: Pristine BN powder was dispersed in IPA at a concentration of 4 mg/mL. The dispersion was probe-sonicated (UH-150A, Auto Science) for 1 h, followed by bath-sonication for 6 h (FB11203, Fisher Brand). The dispersion was then centrifuged at 3500 rpm for 30 min and decanted immediately. The concentration of the obtained BNNS dispersion was about 0.4–0.6 mg/mL.

2.3. Preparation of aramid nanofibers suspension (ANFs)

The ANFs/DMSO dispersion was prepared using the method reported by Kotov's group [17]. ACFs (1.0 g) and KOH (1.5 g) were added into 500 mL of DMSO. The suspension was magnetically stirred for 1 week at room temperature, yielding a dark-red ANF suspension (2 mg/mL). It is worth noting that making large pieces of KOH into smaller pieces can shorten the preparation time to 3–4 days. If the KOH is not completely dissolved, the suspension will be darker.

2.4. Fabrication of nanocomposite film

The ANFs were dialyzed in DI water for 6 h and flocculation was generated. The suspension was stirred for 10 min with a magnetic stirrer. The BNNS/IPA dispersion was then dropped into ANF suspension and placed in a bath sonification for 5 min to form a uniform BNNSs/ANFs dispersion. The prepared BNNSs/ANFs dispersion was then vacuum-filtered on a nylon filter membrane (47 mm diameter, 0.2-μm pore size). The obtained wet film was placed between PTFE film and vacuum-dried at 80 °C and followed by pressing in 10 MPa and 180 °C conditions for 5 min.

2.5. Characterization

The morphologies of the BNNSs and ANFs were observed by transmission electron microscopy (TEM) (JEOL1400F) and atomic force microscopy (AFM) (Bruker Instruments, Germany). The film morphologies were tested with a field-emission scanning electron microscopy (FESEM) with an accelerating voltage at 5–10 kV. The mechanical strength of the films was measured using a universal tensile tester (Instron 5565, Instron instruments Inc. USA). Samples were cut into strips with dimensions of 15.0 mm × 10.0 mm. The electric conductivity of the films was tested using an Electro chemical workstation (ZAHNER Elektrik, Germany). A thermogravimetric analyzer (TGA) (TA Q500, USA) was used to analyze the thermal properties of the pure films and the composite films. TGA measurements were carried out at 10 °C/min under an air purge at a flow rate of 20 mL/min, over a temperature range of 20–700 °C. The thermal diffusivity (α) and the heat capacity (Cp) of the samples were determined by a laser flash method (LFA447 Nanoflash). The film density (ρ) was measured according to its volume and mass. The sample was cut into a 12.7-mm-diameter circle at thermal diffusivity test. The thermal conductivity (λ)

was calculated from the measured diffusivity using equation (1):

$$\Lambda = \alpha \cdot \rho \cdot Cp. \quad (1)$$

The relative dielectric permittivity and dielectric loss tangent (tan δ) of the prepared samples were measured by an impedance analyzer (Novo control Concept 80, NOVOCONTROL, Germany) within the frequency range from 10^6 Hz–10^9 Hz. The thermal expansion of the samples in the temperature range from 30 to 250 °C was tested using thermomechanical analysis (TMA) (Model TMA 402 F1/F3 Hyperion, NETZSCH, Germany) at a heating rate of 5 °C/min and a preload force of 0.02 N.

3. Results and discussion

3.1. Process for preparing nanocomposite films and principle analysis

The nanocomposite films were prepared by the process shown in Fig. 1. By deprotonation of the amide groups in a solvent system of DMSO/KOH, The hydrogen bonding interactions in the polymer chains reduced sharply when the ANFs were obtained from ACFs [22]. Compared to the hexagonal boron nitride (h-BN), the exfoliated BNNSs has a higher percentage of hydroxyl groups (-OH) [23]. Then, the ANFs/DMSO dispersion was dialyzed in DI water to assemble ANF building blocks into the gel networks through partial re-protonation to re-implement part of the hydrogen bonding between ANFs [24,25]. As a result, the ANFs could better mix and disperse with BNNSs and form a continuous film. The prepared BNNSs/ANFs dispersion was vacuum-filtered on a nylon filter membrane and then placed between PTFE films and vacuum-dried followed by hot pressing. As a result, films with flexible strength and good thermal conductivity were obtained. The properties including thermal conductivity, electric conductivity, dielectric and mechanical strength of nanocomposite films were then investigated.

3.2. Properties of nanocomposite films

The macroscopic-scale fibers were split into the ANFs, with a width range from 30 to 70 nm and a length of about several micrometers, as measured by FE-SEM, AFM, and TEM (Fig. 2b, c, and d), and yielded a stable and red dispersion of ANFs/DMSO (Fig. 2a). The exfoliated BNNSs were obtained in IPA via ultrasonic treatment based on a pristine BN dispersion with a concentration of 4 mg/mL. The dispersion is stable over periods of hundreds of hours (Fig. 2e). The obtained BNNSs vary in thickness from a few to several layers with a typical lateral size of 100–3000 nm (Fig. 2f, g, and h). Fig. 2f illustrates a BNNSs film structure with 3-nm thickness (less than 10 layers) and 3000-nm width. The TEM sample was taken directly from the as-fabricated dispersion. It contained large quantities of ultrathin 2D nanosheets (Fig. 2g and h). Fig. 2g shows large quantities nanosheets with sizes ranging from 50 to 200 nm and the corresponding selected area electron diffraction (SAED) pattern, demonstrating that the exfoliated BNNSs have a six-fold symmetry.

A pure nano-aramid film with some degree of transparency was prepared by ANFs flocculation. Compared to macroscopic-scale aramid fibers, ANFs have many excellent properties, such as high surface activity, high specific surface area, and excellent mechanical properties [26–28]. The ANFs exhibit high reactivity and can act as high-performance polymeric building blocks [18]. To form the continuous and flexible film shown in Fig. 3a, it is necessary to control the hydrogen bonding between aramid nanofibers. The hydrogen bonding interactions in the polymer chains reduce sharply after deprotonation procedure. It is worth noting that the reactive ANF building blocks could be assembled into the networks of the ANFs through a partial re-protonation procedure to re-implement part of the hydrogen bonding between aramid nanofibers. As a result, the ANFs could better mix and disperse with BNNSs and form a continuous film. The BNNSs/ANFs nanocomposite film exhibits a lamellar structure with interspersed BNNSs, as observed in the SEM images of the cross section (Fig. 3h and i). The cross-sectional image shows that the 2D nanosheets are tightly stacked in the nanofiber networks and that the layered structure is well-preserved in the film's cross section. The surface morphology images (Fig. 3e and f) show that the BNNN are thin sheets, which bond to each other and form a continuous plane network structure. All of these structures shed light on the high thermal conductivity, mechanical strength, and low dielectric permittivity properties shown in Fig. 4 and Fig. 5.

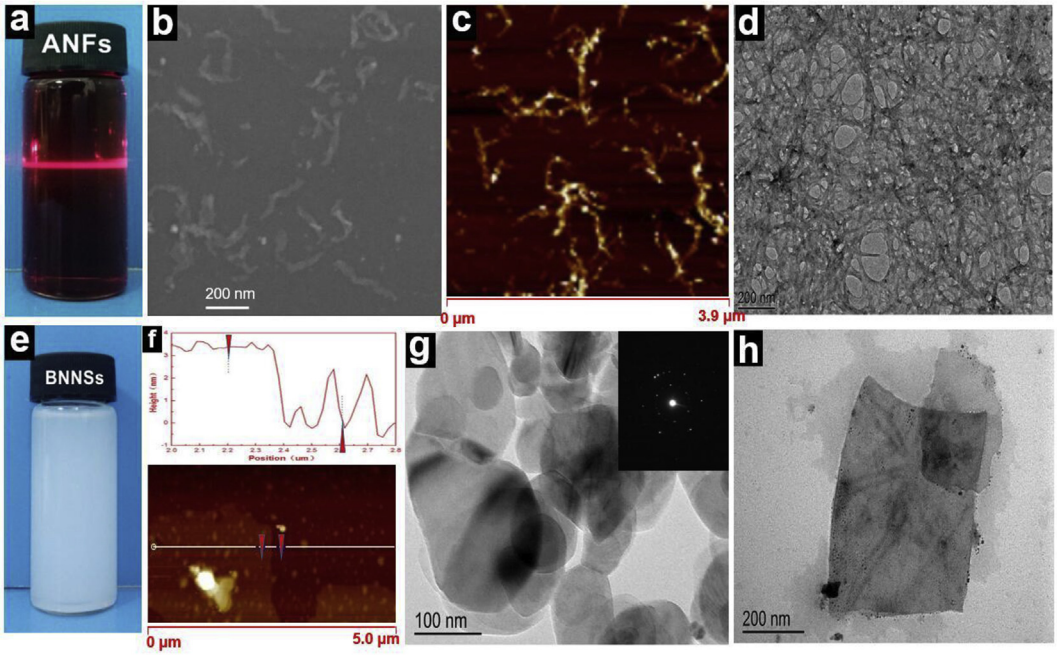

Fig. 2. (a) Digital photo, (b) SEM image, (c) AFM image, and (d) TEM image of ANFs; (e) Digital photo of BNNSs dispersion; (f) AFM of BNNSs; (g) TEM image of ultrathin BNNSs and the corresponding SAED pattern; (h) TEM image of BNNSs.

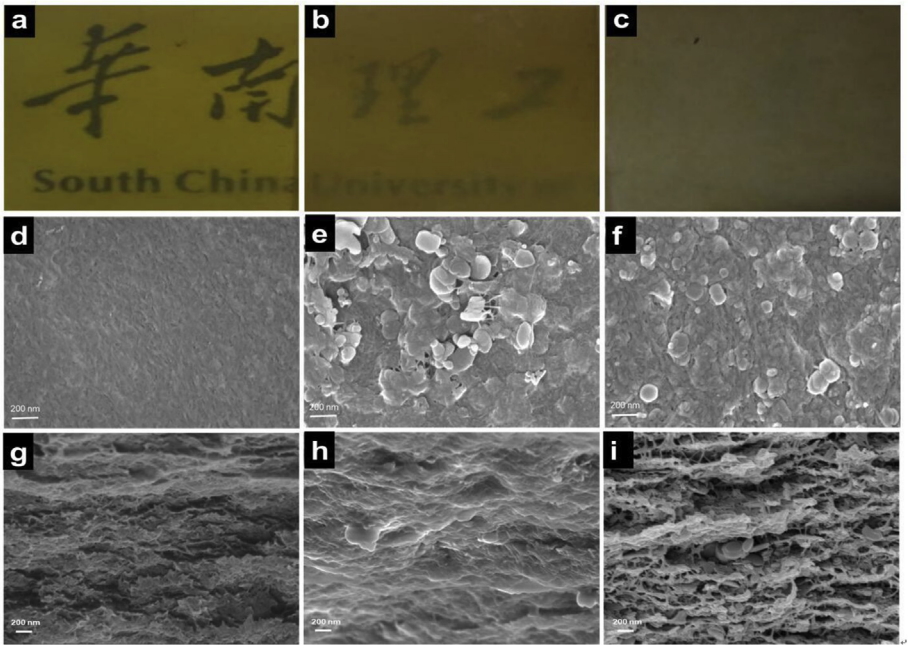

Fig. 3. (a) Image of pure aramid nanofilm and nanocomposite films with 30 wt% (b) and 50 wt% (c) of BNNSs; (d) SEM surface morphology images of pure aramid nanofilm and nanocomposite films with 30 wt% (e) and 50 wt% (f) of BNNSs; (g) SEM cross section images of pure aramid nanofilm and nanocomposite films with 30 wt% (h) and 50 wt% (i) of BNNSs.

The nanocomposite film with 30 wt% BNNSs shown in Fig. 4a presents good flexibility. The current-time curves of nanocomposite films are illustrated in Fig. 4b. It is clear that the current passed is small enough to be negligible, which means the films are insulated. Specifically, the variation trend of electric conductivity in Fig. 4b is consistent with the dielectric loss tan δ in Fig. 5b, in line with Wu's research [29]. The strain-stress curves for the nanocomposite films with different BNNSs loadings are illustrated in Fig. 4c, while the comparison of tensile strength of nanocomposite films are illustrated in Fig. 4d. The average tensile strength of the samples with 0, 10, 15, 30, 45, 50 wt% BNNSs were 125.38 MPa, 103.65 MPa, 87.48 MPa, 71.85 MPa, 69.61 MPa and 61.88 MPa, respectively. The standard deviation of tensile strength was 5.56 MPa, 2.95 MPa, 1.39 MPa, 0.46 MPa, 1.82 MPa and 0.39 MPa respectively. It can been seen that the tensile strength reduced with an increase of BNNSs mass percent. The sample with 50 wt% BNNSs has relatively weak strength is caused by multiple interactions between ANFs and BNNSs. Here, it is believed that the appropriate spacing of amide groups of ANFs makes possible the presence of multiple interfacial hydrogen bonds and the existence of π-π interactions between ANFs, which contributed to the tensile strength of the films [30,31]. The accumulation of BNNSs during vacuum filtration brought relatively weak interfacial interactions such as π-π interactions and reduce the interfacial area among ANFs. An observation from Fig. 3i can be direct evidence. For the nanocomposite films, it is believed that the much greater bond strength in hydrogen bonding should play a dominant role, though other non-bonding interactions such as van der Waals forces may also contribute to the film strength [32,33]. Compared to the BNNSs nanofilm, which is difficult to peel off from the filter paper, the introduction of ANFs can tailor the mechanical performance of the pure BNNSs nanofilm. At the same time, compared to the pure nano-aramid film with a thermal conductivity of 0.1325 ($w{\cdot}m^{-1}{\cdot}k^{-1}$), the introduction of BNNSs can effectively improve the thermal conductivity of the film. As shown in Fig. 4e, the composite film possesses an out-plane thermal conductivity of up to 0.6156 ($w{\cdot}m^{-1}{\cdot}k^{-1}$) at 50 wt% BNNSs, a conductivity almost 5 times greater than pure nano-aramid film, which is attributed to the homogenous dispersion of the high thermal conductivity BNNSs causing phonon scattering of propagating heat flux. Fig. 4f shows both the tensile strength and the thermal conductivity of composite films with different BNNSs loadings. This allows for the tailoring of the mechanical and thermal conductive performance of the film.

The high-frequency dielectric properties and coefficient of thermal expansion (CTE) of the nanocomposite films are shown in Fig. 5. The dielectric permittivity and tan δ of the nanofilms within the frequency range from 1.0 MHz to 1.0 GHz at room temperature are shown in Fig. 5a and b, respectively. The results reveal that the dielectric permittivity of the nanofilms increases with the increased loading of BNNSs. This increase can be easily interpreted as the effect of interspersed BNNSs and the micropores in the film. Furthermore, it can also be seen from Fig. 5a that the dielectric permittivity of the films remains approximately constant up to nearly 1 GHz and then decreases sharply. Studies have reported that space charge polarization is considered as the dominating polarization mechanism at the low-frequency regime (below 1 MHz). The permittivity approaches a constant value with frequencies beyond 10^5 Hz [34,35]. From Fig. 5a, the sharp decrease close to 1 GHz indicates that the relaxation of electronic polarization is the dominating polarization mechanism within the frequency range from 1.0 MHz to 1.0 GHz. The tan δ exhibit the same tendency with dielectric permittivity and is dependent on the variation of frequency, which complied with the common behavior of polymer composites in other research [36,37]. Here, the tan δ of the nanofilms decreases with increasing frequency, is relatively stable around 10^8 Hz, and sharply decreases close to 1 GHz (Fig. 5b). The dielectric dissipation factor tan δ of a polymer or material is one of the key electrical properties and determines whether the polymer or material is suitable in many applications such as in the insulation of cables, encapsulates for electric components, interlay dielectrics, and printed wiring board materials. It is the function of frequency, temperature, and material properties [38]. In the high frequency region ($> 10^5$ Hz), with the frequency increased, only the electron polarization can keep up with the change of the electric field, and the dipole orientation polarization can't be carried out. As a result, the dielectric constant reduced to a value that only contributed by the atomic polarization and electron polarization. The same, dielectric loss reduced to a small value [39,40]. In addition, with an increase of BNNSs mass percent, the tan δ of the nanofilms increases due to the existence of air-gap between ANFs and BNNSs. The permittivity of low dielectric films is usually measured at a frequency of 1 MHz, so the permittivity and tan δ at 1 MHz are independently stated in Fig. 5c. The maximum dielectric permittivity of the nanocomposite films is < 2.7, which is almost as good as ultra-low dielectric constant

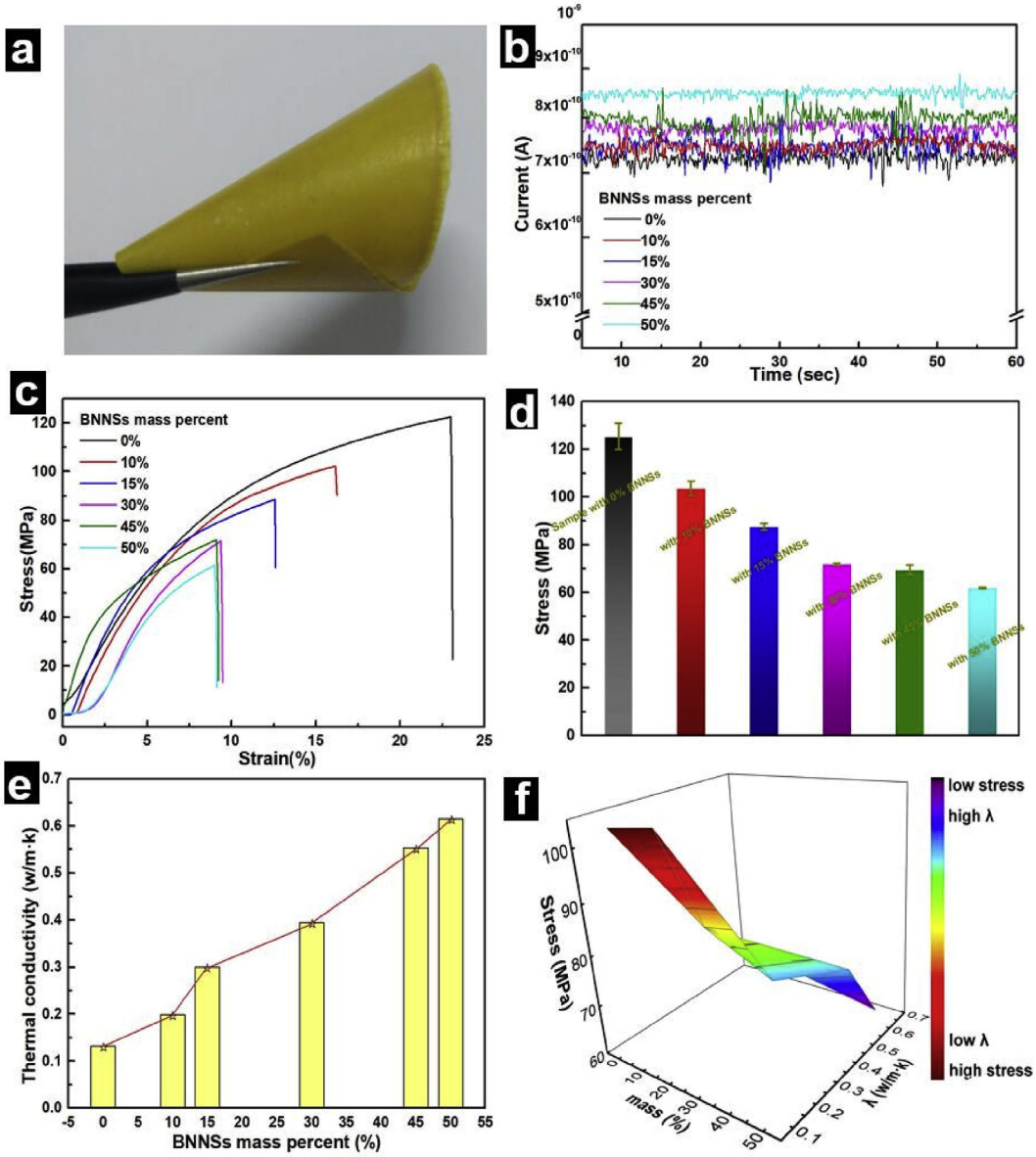

Fig. 4. (a) Sample with 30 wt% BNNSs; (b) The current-time curve of nanocomposite films; (c) The stress-strain curve of nanocomposite films; (d) The comparison of tensile strength of nanocomposite films; (e) The out-plane thermal conductivity of nanocomposite films; (f) Mechanical properties and thermal conductivity of nanocomposite films with different BNNS loadings.

materials, while the $\tan\delta < 0.05$. Furthermore, the coefficient of thermal expansion (CTE) of pure aramid nanofilm and nanocomposite films is measured in the temperature range of 30–250 °C as it is also one of the important properties for electronic application, especially for high-frequency and high-speed substrates. Fig. 5d reveals that the CTE of the nanofilms decreases with the increased loading of BNNSs. This decrease can be interpreted by observing the clear laminar structure in the films, corresponding to the cross section shown in Fig. 3. The filtration process is similar to the layer assembly structure, with the space between layers being large due to the increasing insertion of BNNSs. When the nano-aramid fibers undergo expansion upon temperature change, the increased dimensionality may occupy the layer space, leading to smaller thermal expansion.

Fig. 6 shows the TGA curves of the nanofilms. Overall, the thermal stability of the pure aramid nanofilm and nanocomposite films is basically the same, as they are relatively stable under high-temperature conditions. The degradation rate decreases with an increase of BNNSs mass percent. It is worth noting that there is a slight degradation rate ranged from 2% to 10% before thermal decomposition, which was due to the existence of some individual unstable-unchained nano-aramid fiber after re-protonation process.

4. Conclusions

In this present study, we report minimally dielectric and highly thermally conductive nano-aramid composite films with boron nitride nanosheets used as heat spreaders for flexible electronics or high-frequency and high-speed substrates. The thermal conductivity of nano-aramid composite films can be tuned by varying the weight percent of BNNSs, reaching values as high as 0.6156 ($w{\cdot}m^{-1}{\cdot}k^{-1}$), which is about 5 times higher than that of the pure aramid nanofilm. The enhanced thermal conductivity originates from the efficient construction of BNNSs thermal conduction pathways or networks, which reduces phonon scattering. In addition, the nanocomposite film has low dielectric constants (~2.4 at 10^8 Hz) along with excellent mechanical flexibility and strength (~62 MPa). We further demonstrate that the

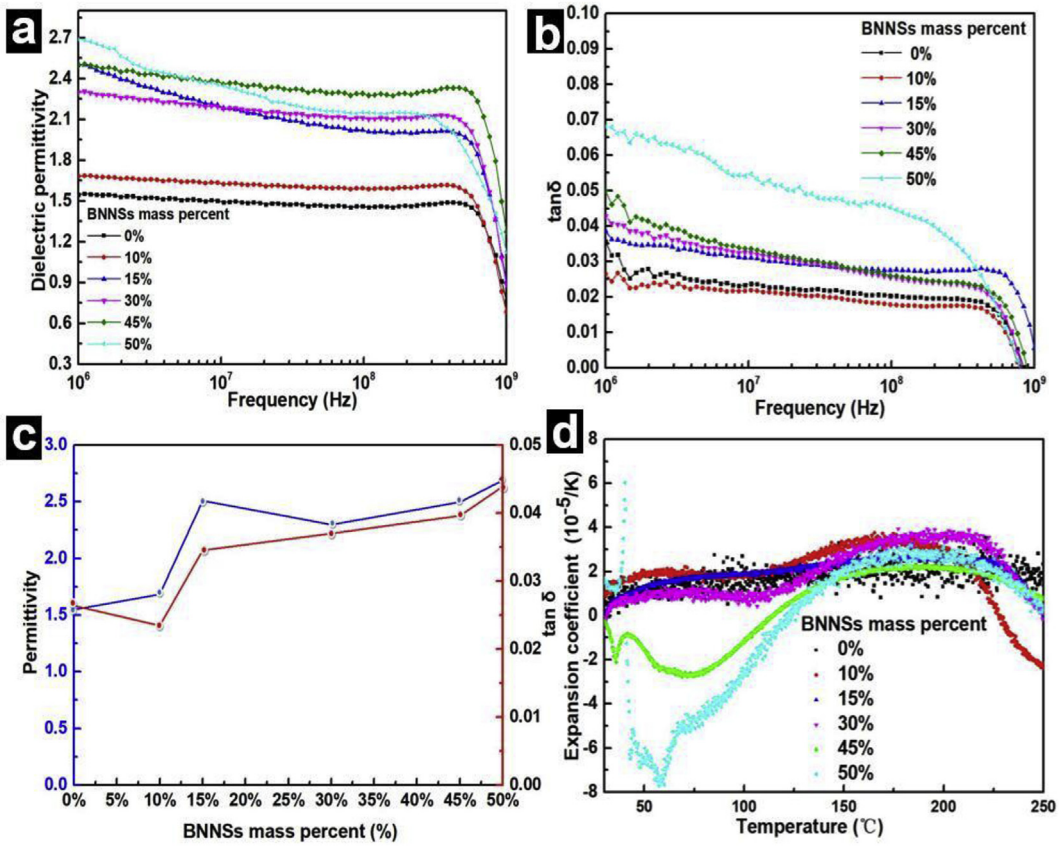

Fig. 5. (a) Dielectric permittivity and (b) tan δ curve of pure nano-aramid film and nanocomposite films at the frequency range from 10^6–10^9 Hz; (c) Dielectric permittivity and tan δ of nanofilms with different BNNS loadings at a frequency of 1 MHz; (d) Coefficient of thermal expansion (CTE) of pure nano-aramid film and nanocomposite films measured in the temperature range of 30–250 °C.

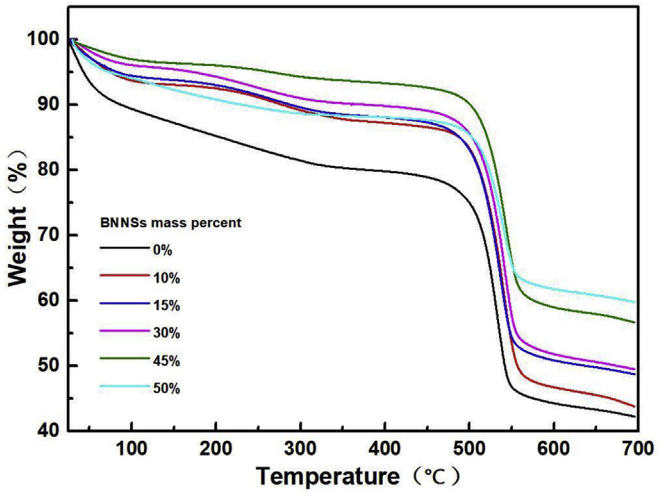

Fig. 6. TGA curves of pure nano-aramid film and nanocomposite films.

CTE of the nanocomposite films with ANFs and BNNSs is smaller than the pure nanofilm. We believe that aramid nanocomposite films with boron nitride nanosheets have the potential to replace conventional plastic and plant-fiber paper substrates in some flexible electronic applications or high-frequency and high-speed communication fields in the future.

Acknowledgments

This work was financially supported by the Guangzhou Science and Technology Plan Project (Grant No. 201704030066), Guangdong Province Youth Science and Technology Innovation Talents (Grant No. 2014TQ01C781), Science and Technology Planning Project of Guangdong Province, China (Grant No. 2016B090918074), and the Fundamental Research Funds for the Central Universities, South China University of Technology (Grant No. 2017ZD087). Guangdong Province Science Foundation for Cultivating National Engineering Research Center for Efficient Utilization of Plant Fibers (2017B090903003).

Appendix A. Supplementary data

Supplementary data to this article can be found online at https://doi.org/10.1016/j.compscitech.2019.02.006.

References

[1] Z. Lin, A. Mcnamara, Y. Liu, K.S. Moon, C.P. Wong, Exfoliated hexagonal boron nitride-based polymer nanocomposite with enhanced thermal conductivity for electronic encapsulation, Compos. Sci. Technol. 90 (2) (2014) 123–128 https://doi.org/10.1016/j.compscitech.2013.10.018.

[2] L. Qin, G. Li, J. Hou, X. Yu, H. Ding, Q. Zhang, N. Wang, X. Qu, Preparation, characterization, and thermal properties of poly (methyl methacrylate)/boron nitride composites by bulk polymerization, Polym. Compos. 36 (9) (2015) 1675–1684 https://doi.org/10.1002/pc.23078.

[3] Q. Li, Y. Guo, W. Li, S. Qiu, C. Zhu, X. Wei, M. Chen, C. Liu, S. Liao, Y. Gong, Ultrahigh thermal conductivity of assembled aligned multilayer graphene/epoxy composite, Chem. Mater. 26 (15) (2012) 4459–4465 https://doi.org/10.1021/cm501473t.

[4] W.P. Ting, F.P. Tseng, K.C. Chiou, Advanced Materials with Low Dielectric Properties and Highly Thermal Conductivity, 345 E IEEE, 47th st, New York, NY 10017 USA, 2017, pp. 430–433.

[5] L. Wu, F. Xiang, W. Liu, R. Ma, H. Wang, Hot-pressing sintered BN-SiO_2 composite ceramics with excellent thermal conductivity and dielectric properties for high frequency substrate, Ceram. Int. (2018), https://doi.org/10.1016/j.ceramint.2018.06.084.

[6] W. Ling, A. Gu, G. Liang, L. Yuan, New composites with high thermal conductivity and low dielectric constant for microelectronic packaging, Polym. Compos. 31 (2) (2010) 307–313 https://doi.org/10.1002/pc.20805.
[7] N. Song, J. Jiao, S. Cui, X. Hou, P. Ding, L. Shi, Highly anisotropic thermal conductivity of layer-by-layer assembled nanofibrillated cellulose/graphene nanosheets hybrid films for thermal management, ACS Appl. Mater. Interfaces 9 (3) (2017) 2924 https://doi.org/10.1021/acsami.6b11979.
[8] Y. Yao, X. Zeng, G. Pan, J. Sun, J. Hu, Y. Huang, R. Sun, J.B. Xu, C.P. Wong, Interfacial engineering of silicon carbide nanowire/cellulose microcrystal paper toward high thermal conductivity, ACS Appl. Mater. Interfaces 8 (45) (2016) 31248 https://doi.org/10.1021/acsami.6b10935.
[9] H. Zhu, Y. Li, Z. Fang, J. Xu, F. Cao, J. Wan, C. Preston, B. Yang, L. Hu, Highly thermally conductive papers with percolative layered boron nitride nanosheets, ACS Nano 8 (4) (2014) 3606–3613 https://doi.org/10.1021/nn500134m.
[10] K. Wu, J. Fang, J. Ma, R. Huang, S. Chai, F. Chen, Q. Fu, Achieving a collapsible, strong and highly thermally conductive film based on oriented functionalized boron nitride nanosheets and cellulose nanofiber, ACS Appl. Mater. Interfaces 9 (35) (2017) 30035 https://doi.org/10.1021/acsami.7b08214.
[11] X. Zeng, J. Sun, Y. Yao, R. Sun, J.B. Xu, C.P. Wong, A combination of boron nitride nanotubes and cellulose nanofibers for the preparation of A nanocomposite with high thermal conductivity, ACS Nano 11 (5) (2017), https://doi.org/10.1021/acsnano.7b02359.
[12] S.K. Swain, S. Dash, C. Behera, S.K. Kisku, L. Behera, Cellulose nanobiocomposites with reinforcement of boron nitride: study of thermal, oxygen barrier and chemical resistant properties, Carbohydr. Polym. 95 (2) (2013) 728–732 https://doi.org/10.1016/j.carbpol.2013.02.080.
[13] Z. Yang, L. Zhou, W. Luo, J. Wan, J. Dai, X. Han, K. Fu, D. Henderson, B. Yang, L. Hu, Thermally conductive, dielectric PCM-boron nitride nanosheet composites for efficient electronic system thermal management, Nanoscale 8 (46) (2016) 19326 https://doi.org/10.1039/c6nr07357c.
[14] C. Jin, X. Huang, B. Sun, Y. Wang, Y. Zhu, P. Jiang, Vertically aligned and interconnected boron nitride nanosheets for advanced flexible nanocomposite thermal interface materials, ACS Appl. Mater. Interfaces 9 (36) (2017) 30909 https://doi.org/10.1021/acsami.7b08061.
[15] J. Li, J. Fan, K. Liao, J. Xie, Y. Chen, P. Liu, Y. Min, Q. Xu, Facile fabrication of a multifunctional aramid nanofiber-based composite paper, RSC Adv. 6 (93) (2016), https://doi.org/10.1039/c6ra15895a.
[16] M. Jiang, Z. Wang, J. Deng, Z. Lu, Structures and properties comparison of meta-aramid and para-aramid fibrid and their paper-based insulation materials, Insul. Mater. (2017), https://doi.org/10.16790/j.cnki.1009-9239.im.2017.01.004.
[17] M. Yang, K. Cao, L. Sui, Y. Qi, J. Zhu, A. Waas, E.M. Arruda, J. Kieffer, M.D. Thouless, N.A. Kotov, Dispersions of aramid nanofibers: a new nanoscale building block, ACS Nano 5 (9) (2011) 6945 https://doi.org/10.1021/nn2014003.
[18] K. Cao, C.P. Siepermann, M. Yang, A.M. Waas, N.A. Kotov, M.D. Thouless, E.M. Arruda, Reactive aramid nanostructures as high-performance polymeric building blocks for advanced composites, Adv. Funct. Mater. 3 (16) (2013) 2072–2080 https://doi.org/10.1002/adfm.201202466.
[19] W. Cao, L. Yang, X. Qi, Y. Hou, J. Zhu, M. Yang, Carbon nanotube wires sheathed by aramid nanofibers, Adv. Funct. Mater. 27 (34) (2017) 1701061 https://doi.org/10.1002/adfm.201701061.
[20] Y. Mo, Q. Liu, J. Fan, P. Shi, Y. Min, Q. Xu, Heterocyclic aramid nanoparticle-assisted graphene exfoliation for fabrication of pristine graphene-based composite paper, J. Nanoparticle Res. 17 (7) (2015) 1–13 https://doi.org/10.1007/s11051-015-3099-x.
[21] J. Li, W. Tian, H. Yan, L. He, X. Tuo, Preparation and performance of aramid nanofiber membrane for separator of lithium ion battery, J. Appl. Polym. Sci. 133 (30) (2016), https://doi.org/10.1002/app.43623.
[22] R.R. Burch, W. Sweeny, H.W. Schmidt, Y.H. Kim, Preparation of aromatic polyamide polyanions: a novel processing strategy for aromatic polyamides, Macromolecules 23 (4) (1990) 1065–1072 https://doi.org/10.1021/ma00206a026.
[23] Y. Lin, T.V. Williams, T.B. Xu, W. Cao, H.E. lsayed-Ali, J.W. Connell, Aqueous dispersions of few-layered and monolayered hexagonal boron nitride nanosheets from sonication-assisted hydrolysis: critical role of water, J. Phys. Chem. C 115 (6) (2011) 2679–2685 https://doi.org/10.1021/jp110985w.
[24] M. Yang, K. Cao, B. Yeom, M. Thouless, A. Waas, E.M. Arruda, N.A. Kotov, Aramid nanofiber-reinforced transparent nanocomposites, J. Compos. Mater. 49 (15) (2015), https://doi.org/10.1177/0021998315579230.
[25] J. Fan, Z. Shi, M. Tian, J. Yin, Graphene–aramid nanofiber nanocomposite paper with high mechanical and electrical performance, RSC Adv. 3 (39) (2013) 17664–17667 https://doi.org/10.1039/c3ra42515k.
[26] B.A. Patterson, M.H. Malakooti, J. Lin, A. Okorom, H.A. Sodano, Aramid nanofibers for multiscale fiber reinforcement of polymer composites, Compos. Sci. Technol. 161 (2018), https://doi.org/10.1016/j.compscitech.2018.04.005.
[27] J. Zhu, M. Yang, A. Emre, J.H. Bahng, L. Xu, J. Yeom, B. Yeom, Y. Kim, K. Johnson, P. Green, Branched aramid nanofibers, Angew. Chem. Int. Ed. 56 (39) (2017), https://doi.org/10.1002/anie.201703766.
[28] J. Fan, J. Wang, Z. Shi, S. Yu, J. Yin, Kevlar nanofiber-functionalized multiwalled carbon nanotubes for polymer reinforcement, Mater. Chem. Phys. 141 (2–3) (2013) 861–868 https://doi.org/10.1016/j.matchemphys.2013.06.015.
[29] K. Wu, Y. Li, R. Huang, S. Chai, F. Chen, Q. Fu, Constructing conductive multi-walled carbon nanotubes network inside hexagonal boron nitride network in polymer composites for significantly improved dielectric property and thermal conductivity, Compos. Sci. Technol. 151 (2017) 193–201 https://doi.org/10.1016/j.compscitech.2017.07.014.
[30] S.R. Kwon, J. Harris, T. Zhou, D. Loufakis, J.G. Boyd, J.L. Lutkenhaus, Mechanically strong graphene/aramid nanofiber composite electrodes for structural energy and power, ACS Nano 11 (7) (2017) 6682–6690 https://doi.org/10.1021/acsnano.7b00790.
[31] J. Zhu, W. Cao, M. Yue, Y. Hou, J. Han, M. Yang, Strong and stiff aramid nanofiber/carbon nanotube nanocomposites, ACS Nano 9 (3) (2015) 2489–2501 https://doi.org/10.1021/nn504927e.
[32] Q. Kuang, D. Zhang, J. Yu, Y. Chang, M. Yue, Y. Hou, M. Yang, Toward record-high stiffness in polyurethane nanocomposites using aramid nanofibers, J. Phys. Chem. C 119 (49) (2015) 27467–27477 https://doi.org/10.1021/acs.jpcc.5b08856.
[33] J. Li, J. Fan, K. Liao, J. Xie, Y. Chen, L. Peng, Y. Min, Q. Xu, Facile fabrication of multifunctional aramid nanofiber-based composite paper, RSC Adv. 6 (93) (2016), https://doi.org/10.1039/C6RA15895A.
[34] T.L. Li, S.L. Hsu, Enhanced thermal conductivity of polyimide films via a hybrid of micro- and nano-sized boron nitride, J. Phys. Chem. B 114 (20) (2010) 6825–6829 https://doi.org/10.1021/jp101857w.
[35] X. Chen, H. Huang, X. Shu, S. Liu, J. Zhao, Preparation and properties of a novel graphene fluoroxide/polyimide nanocomposite film with a low dielectric constant, RSC Adv. 7 (4) (2017) 1956–1965 https://doi.org/10.1039/c6ra25343a.
[36] F. Han, S. Ren, J. Deng, T. Yan, M. Xing, B. Peng, L. Liu, Dielectric response mechanism and suppressing high-frequency dielectric loss in Y 2 O 3 grafted $CaCu_3Ti_4O_{12}$ ceramics, J. Mater. Sci. Mater. Electron. 28 (4) (2017) 1–10 https://doi.org/10.1007/s10854-017-7671-2.
[37] W. Li, Z. Song, Q. Jing, Z. Tan, H. Chu, X. Wu, N. Wei, Largely enhanced dielectric and thermal conductive properties of novel ternary composites with small amount of nanofillers, Compos. Sci. Technol. 163 (2018) 71–80 https://doi.org/10.1016/j.compscitech.2018.05.008.
[38] X. Yu, Y. Bing, L. Fang, X. Wang, Prediction of the dielectric dissipation factor tan δ of polymers with an ANN model based on the DFT calculation, React. Funct. Polym. 68 (11) (2008) 1557–1562 https://doi.org/10.1016/j.reactfunctpolym.2008.08.009.
[39] J.H. Ahn, H.S. Lee, D.S. Seo, K.U. Jang, W.J. Lee, T.W. Kim, Dielectric properties depending on frequency in organic light-emitting diodes, Thin Solid Films 516 (9) (2008) 2626–2629 https://doi.org/10.1016/j.tsf.2007.04.158.
[40] P. Kumar, M. Kar, Effect of structural transition on magnetic and dielectric properties of La and Mn co-substituted $BiFeO_3$ ceramics, Mater. Chem. Phys. 148 (3) (2014) 968–977 https://doi.org/10.1016/j.matchemphys.2014.09.007.